

FIGURE CONTROL FOR A SEGMENTED TELESCOPE MIRROR

Terry S. Mast and Jerry E. Nelson

Lawrence Berkeley Laboratory, Berkeley, California 94720

March 1979

ABSTRACT

We have studied the properties of a system to control the figure of a large telescope primary mirror that is composed of many individual segments. The geometry considered, employing hexagonal mirrors, allows a simple and economical control system. The system is shown to be reliable and effective in continuously maintaining the figure to the precision required for optical astronomy.

NOTICE

This report was prepared as an account of work sponsored by the United States Government. Neither the United States nor the United States Department of Energy, nor any of their employees, nor any of their contractors, subcontractors, or their employees, make any warranty, express or implied, or assume any legal liability or responsibility for the accuracy, completeness or usefulness of any information, apparatus, product or process disclosed, or represent that its use would not infringe privately owned rights.

CONTENTS

I.	Introduction	1
II.	Mirror and Control System Design	4
III.	Control Program	8
IV.	Sensor Noise	11
V.	Actuator Noise	15
VI.	Sensor Failures	16
VII.	Real Time Control	18
VIII.	Summary	19

I. INTRODUCTION

The cost of large primary mirrors for astronomical telescopes can be greatly reduced by using an assembly of small mirror segments instead of one large solid mirror. The cost of producing small mirrors is less and the risk of catastrophic breakage is virtually eliminated. The weight of the total mirror can also be reduced, allowing a simplified and less expensive support structure. In addition fabrication and handling equipment such as aluminizing tanks and cranes can be substantially reduced in scale and cost.

The central problem with a segmented primary is to assemble the small mirrors and maintain their orientations and positions so they form the figure of a single large optical quality mirror. We describe here the study of a proposed control system for a mirror composed of many hexagonal elements. Our analysis shows that the design considered is both feasible to construct and reliable. It is feasible to construct in the sense that mirror sensors and mirror displacement actuators are capable of producing images of good optical quality. It is reliable in the sense there is sufficient redundancy that the continuous figure control operates even if some components should fail and the overall alignment and calibration of the system is not lost should there be a power failure.

This analysis is part of a much larger project to design a fully steerable ten meter telescope for the University of California.¹ Several designs including both segmented and monolithic primary mirrors are being considered. The broader goals of the design include: image quality that is limited by atmospheric

seeing, not by optical aberrations; a wide angular field (about 20 minutes); capability for observations from 0.3 to 30 microns; reliability; and of course economy in construction and operation. Other designs and details of other aspects of the design considered here will be described in other publications. These will include an overview of the segmented design² and descriptions of mirror segment fabrication; the design, production, and testing of mirror sensors and actuators; alignment procedures; and mirror support.

The control system is used to monitor the figure of the primary mirror (once it is established) and to continuously preserve it against distortions induced by wind, gravity loading, and temperature changes. In the past control systems using the center of curvature for interferometric sensing of the mirror figure have been used successfully.³ However, to limit the size of the telescope structure we have avoided requiring access to the center of curvature. Systems employing starlight are also feasible and sensing could then be done at the focus.⁴ However, the desire to observe in daylight and a rather limited angular field make this technique unattractive. Other techniques employing light beams reflected from the mirror surface are possible, but since many astronomical measurements require extremely low background light levels we felt it advantageous to avoid shining any light on the mirror surface. As a consequence we have explored techniques which monitor the mirror position without using the front surface.

The system chosen uses three actuators on the back of each segment to control the orientation and position, and it uses displacement

sensors on the back at the adjacent edges of the segments. In Section II we describe the geometry and the assumed sensor and actuator characteristics. The algorithm for using the sensor information to control the orientation of the segments is described in Section III. Using this algorithm we then establish the relationship between sensor and actuator precision and image quality (Sections IV and V). The image quality is first studied with geometrical optics and then with diffraction theory to describe the image as a function of wavelength. In Section IV we describe tests of the system's sensitivity to sensor failures. Section VII briefly discusses the practical implementation of a real time control system. Finally, in Section VIII we summarize our results and discuss the general applicability of this method to other segmented designs.

II. MIRROR AND CONTROL SYSTEM DESIGN

By design the primary mirror will be an assembly of small stiff segments. In choosing a particular segment geometry we have tried to minimize the number of surface shapes, the number and complexity of control elements, and the number of different types of components. These objectives have led to the hexagonal design shown in Figure 1. The mirror consists of a central reference mirror surrounded by three "rings" of hexagonal segments with a total of 54 segments. Each segment has 0.70 meter edges with the area of the assembly being equal to that of a ten meter diameter circular mirror. This design requires only one shape for the segment mirror blanks. Other configurations such as annular rings of "rectangular" segments offer other advantages. However, as will be shown, hexagons have a natural "interlocking" geometry which greatly simplifies the requirements for the control system. For this study we have assumed the figure to be a paraboloid with focal ratio $f/1.5$. (The exact figures of the primary and secondary for the 10 meter telescope are still to be determined.) This design employs 9 different off-axis paraboloidal sections. Techniques for fabricating these off-axis surfaces are being developed and tested.

The control system needs to sense the location and orientation of the segments and move them to maintain the desired surface. Our general approach has been to keep the front surface free of obstructions by placing the sensing and actuating control elements on the back of the segments. This preserves the large collecting area and avoids additional light sources and scattering surfaces. The goal was to produce images either limited by atmospheric

seeing or by diffraction. For wavelengths beyond 10 μm we expect diffraction effects to dominate the image quality. The system needs to provide rapid and continuous control in the presence of variable loading due to wind, gravity, etc. In addition it should be insensitive to the effects of power failures and defective components. Since it must operate all the time it must perform reliably, be easily monitored, and be readily maintained.

Each mirror segment has six degrees of freedom. We characterize these as focus, rotation about two axes in the segment plane or "tilt", rotation about the normal to the segment, and finally radial and azimuthal motion of the segment center in the surface of the primary mirror. We assume in this study that only the first three motions are in need of active control. The remaining three motions will be constrained by inward compression on the entire mirror assembly or by the rigidity of the support structure.

The orientation of each segment is controlled by three displacement actuators arranged in a triangle on the back of the segment (see Figure 2). In practice the three actuators are attached to the segment through a 9 support point assembly. There are a total of 162 actuators of identical construction. A possible design for the actuator employs a roller screw driven by a torque motor. Details of this design and tests of the roller screw performance are described in reference 5. Initial estimates indicate these assemblies will be economical and will provide rapid positive control with a noise level less than 0.05 μm . Shaft encoders will allow precise changes of the actuator length in response to the information from the sensors.

There are 288 sensors overlapping the edges of the mirrors (Figure 3). Each sensor measures locally the differences in heights of the surfaces of the two adjacent mirrors. By design these sensors will be sensitive to displacements normal to the mirror surface, and extremely insensitive to displacements in the plane of the mirror or to any rotation or tilt about the center of the sensor. No direct tilt measurements of the segments are made. The "interlocking" character of the hexagonal geometry allows the orientation (the three degrees of freedom) of all segments to be determined from these displacement measurements.

This interlocking character is illustrated in Figure 4 showing a small section of the inner ring of segments. The corner of the segment fitting into the indentation in the central mirror allows the measurement of the segment's orientation with respect to that of the central mirror. The four measurements of the mirror surface displacements (Figure 4b) can be used to calculate that orientation. In particular, tilt of the mirror is measured by using the segment's stiff lever arm to convert positional information to angular information. The complete geometry of Figure 1 shows that this keystone effect allows the measurement of the six segments which have corners fitting into the central reference mirror. These six segments are most directly coupled to the reference mirror and we label them type 1 (Figure 5). These six then in turn provide indentations for the six segments remaining in the inner ring and we label these type 2. This same procedure is repeated to define successively the orientation of all segments. The degree of direct coupling to the reference decreases from mirror type to mirror type. The final mirror type 7 is the farthest removed from

the central mirror and knowlege of its orientation relies on the many intervening sensors.

The specific sensors under consideration will measure the relative heights of the two surfaces by a ratiometric capacitance technique. Initial calculations assuming low thermal expansion glass blocks for the capacitor plates and a bridge curcuit indicate that displacement uncertainties of $0.05 \mu\text{m}$ or better can be achieved. Details of the design and prototype testing are described in reference 5. The use of only one type of sensor and the simplicity of its design are features giving reliability to the system.

Since there are many more sensors than actuators the system is highly redundant. The three extra sensors per mirror provide both increased precision and stability. The redundant sensors also allow cross checks of sensor performance and the extra information needed so that individual failures do not disable the system.

III. CONTROL PROGRAM

The control program uses the sensor readings to determine the desired actuator motion and thus adjust the mirror orientations in response to perturbations from the wind, temperature changes, and changes in the gravity loading of the support structure with steering. We emphasize here that the control system does not provide the initial alignment of the segments. A technique and the optical elements required for it will be described in a future publication. In addition a technique for periodic calibration of the sensors and actuators using stellar images will be described. For this paper we assume the alignment has been achieved and the control system described here is used to maintain that alignment.

For the purposes of this study and without loss of generality we assume that when the mirrors are correctly oriented all of the sensors read zero. (In practice one will analyze the difference between the measured value and the desired one.) Perturbations then change the orientation of the segments and generate non-zero sensor readings. In the geometrical optics limit (zero wavelength) each segment of the paraboloid will make its own spot stellar image and the final image will contain 55 individual spots. Without perturbations or errors these will all superpose to form a single stellar image. With perturbations and errors a distribution of spots will be formed and the rms radius of this distribution is one measure of the image quality and control system performance.

The segment-sensor system is a complex coupled array and all sensors contribute some information about the orientation of each segment. Thus the calculation of the desired motion of the actuators relies on solving a set of coupled equations using all of the sensor measurements.

We have used a chisquare minimization technique to optimally use all of the information. Each sensor reading is linearly related to the lengths of the actuators on the adjacent mirrors.

$$s_j^{\text{exp}} = \sum_m A_{jm} p_m \quad 1.$$

where s_j is the expected sensor reading of the j^{th} sensor and p_m are the actuator lengths. The matrix A_{jm} is defined by the geometry and for the 54 segment system of Figures 1-3 the matrix has 288 x 162 elements. However, since each sensor measurement depends only on the lengths of the six actuators on the two defining mirrors, most of the elements of the matrix are zero.

The chisquare is then defined

$$\chi^2 = \sum_j \frac{(\sum_m A_{jm} p_m - s_j)^2}{(\sigma_j)^2} \quad 2.$$

where s_j are the measured sensor readings and σ_j their errors. The set p_m which minimizes χ^2 is the solution to these 162 coupled linear equations. The exact solution is found by effectively inverting A and has the form

$$p_k = \sum_m B_{km} s_m \quad 3.$$

where the matrix B is completely defined by the geometry and the σ_j and does not depend on the s_m . In principle one finds the matrix B from A and σ_j just once for the system. Then for each set of sensor values generated by the perturbations (and noise) only the matrix multiplication of equation 3 is needed to calculate the desired actuator movements. In the computer simulation of the control system described below we have used the very efficient algorithm of Golub and Reinsch⁶ to find the matrix B.

IV. SENSOR NOISE

Even without perturbations of the segments the sensors will have some intrinsic noise which will cause the control program to move the actuators and degrade the image from the ideal. Since the system is linear the rms image size will be proportional to the rms sensor error. Using the dimensions of Figures 1-3 and an assumed sensor noise level of $0.05 \mu\text{m}$ we expect the rms image size to be roughly given by $2(0.05 \mu\text{m})/(0.35 \text{ m}) = 0.06$ arcseconds, where the factor of 2 and 0.35m account for the ratio of the angular image motion to the angular mirror motion and the effective keystone lever arm. For long wavelength observations or techniques such as speckle interferometry the correct phasing (focus degree of freedom) as well as the tilt of the segments is important. We can expect the displacements of the segment centers to be roughly on the scale of an average radius times the average tilt angle = $(2/3)(5 \text{ m})(0.03 \text{ arcseconds}) = 0.5 \mu\text{m}$.

Of course all segments are not alike in their contributions to the image error. The orientations of the segments in the outer rings are less precisely known since they are based on the large number of sensors between that ring and the reference mirror. Roughly speaking the effects of sensor noise may be expected to add in quadrature since they are independent and uncorrelated. Thus the contributions to the rms image size are expected to increase roughly as the square root of the mirror type or "distance" from the central mirror.

We have used the control system program to study these effects quantitatively. The segments were assumed to be in their ideal orientation and random sensor noise was generated with a gaussian

distribution of width $\sigma = 0.05 \mu\text{m}$. The best fit for the actuators was calculated and the image formed by these actuator lengths was analysed. Figure 6 shows a typical spot diagram. The procedure was repeated with 100 sets of random sensor errors to obtain smooth distributions. The image distribution, a superposition of 100 spot diagrams, is given by

$$P(\theta) \theta d\theta d\phi = \frac{1}{2\pi\delta^2} \exp(-\theta^2/2\delta^2) \theta d\theta d\phi \quad 4.$$

The parameter δ , the one dimension gaussian width, is $1/\sqrt{2}$ times the rms radius of the two dimensional distribution.

For the dimensions of Figures 1-3 we found the parameter to be given by $\delta = 1.3 \sigma$, where δ is in arcseconds and σ is in μm . Primary mirrors composed of 1, 2, and 4 rings were also investigated and the results are shown in Figure 7. The important and encouraging feature is the slow rise in δ as the number of rings increases. The conclusion is that with the assumed sensor noise level it is possible to build very large primary mirrors and still have the image quality effectively undegraded by the sensor errors. Extrapolating to 16 rings gives a δ of 0.2 arc seconds. With segments of the size proposed here 16 rings would make a mirror about 40 meters in diameter.

The images formed by the segments of each type were also analyzed. The rms image radius increased from type to type as expected from the decreasing direct coupling to the central mirror. The behavior of δ as a function of mirror type and for the different size primaries is shown in Figure 8. There is a small decrease in δ for a given mirror type as more rings are added since more sensors impose additional constraints.

For the spot distribution (equation 4) the enclosed energy in a circle of radius θ is given by $1 - \exp(-\theta^2/2\delta^2)$. The image radii which contain 80% and 90% of the energy are $\theta(80\%) = 1.8 \delta$ and $\theta(90\%) = 2.1 \delta$. Thus a sensor noise level of $0.05 \mu\text{m}$ gives an image distribution with 80% of the energy in a circle of radius 0.11 arcseconds.

A useful measure of the correct average phasing of the mirrors is the rms surface error. We define this as the rms deviation of the controlled surface from the ideal surface weighted by the area. Its behavior with mirror type and the number of rings is shown in Figure 9. For a three ring primary the rms surface error is $0.3 \mu\text{m}$. Conceptually we can divide the contributions to the rms surface error into two parts; one from the tilting of the segments and one from the overall displacement of the segment center. A comparison of the surface errors with those expected from pure tilting shows the surface errors are primarily due to the overall displacement. The surface errors increase roughly linearly with mirror type as is expected from the square root behavior of the tilt angles.

All of the above analysis used geometrical optics assuming the wavelength of light to be negligible. To understand the effects of discrete steps in the surface the analysis was repeated using the diffraction theory of aberrations (Ref. 7). The best fit actuator solution for each set of random sensor noise gives a specific surface for the primary. This surface was used in a Kirchoff-Fresnel integral to calculate the image plane distribution taking into account the interfering contributions from each differential area of the mirrors. The final image distribution was characterized by the radius containing 80% of the energy. The calculation was based on the procedure described in Born and Wolf and used the expression for the diffraction pattern of a hexagonal aperture of Shack (Ref. 8). The coma for the assumed paraboloidal mirror was included and it increased the calculated image sizes by about 8%. Assuming again a sensor noise level of $0.05 \mu\text{m}$ the parameter $\theta(80\%)$ was calculated and it is plotted as a function of wavelength in Figure 10.

For small wavelengths the 80% radius matches that expected from geometric optics. As the wavelength increases each spot of the spot diagram becomes a diffraction pattern for an individual segment and the 80% radius increases. As the wavelength becomes much larger than the rms surface error the image approaches the diffraction pattern of the whole primary.

V. ACTUATOR NOISE

Following a procedure similar to that used for the sensor noise we have calculated the effect of actuator noise on the image. The noise in a sensor effects more than one segment and thus contributes in a coupled way to the final image quality. Noise in an actuator however effects only one segment and thus the effect on the image quality is more simply calculated. The rms image radius is proportional to the rms actuator position error and for the assumed design we find δ (arcseconds) = $0.68 \times \Delta p$ (microns). The rms surface error is given by the expression dS (microns) = $0.94 \Delta p$ (microns). For actuator errors of 0.05 microns the rms image error is 0.034 arcseconds and the rms surface error is 0.047 microns. The contributions from sensor noise and actuator noise can be added in quadrature and for the design of Figures 1-3 they give a total rms image radius of 0.072 arc seconds.

VI. SENSOR FAILURES

Using geometrical optics we have investigated the effects of sensor failures. Since the sensor designs being considered are simple in construction and expected to be reliable, the number of sensor failures in practice is expected to be quite small.

We have calculated the image degradation when randomly chosen sets of sensors are eliminated from the system. After choosing the sensors to delete, one recalculates the B matrix and performs the same analysis previously described. The degradation of the image increases slowly with the number of sensors eliminated and for a system with 25 sensors eliminated the rms image size is increased by only 10 to 15%.

Eliminating specific sensors instead of random ones also showed the system to be remarkably stable. Removing six sensors (out of 12) at the indented corners of the reference mirror produced only a 10% increase in the image radius. Even removing all sensors between the inner ring and the central mirror except 6 adjacent ones degraded the image by only a factor of 4. We conclude that the multiple ways the segments are related through the sensor array and the large sensor redundancy combine to form a very stable system of control.

In practice, defective sensors can be identified by monitoring each sensor's contribution to χ^2 . If a sensor's average contribution substantially exceeds its expected value, it is labelled as defective. The A matrix is then reconfigured without the suspect sensor and the B matrix is calculated. This reconfiguration will probably take a longer time than the control cycle time of about 0.1 seconds. During this reconfiguration the sensor reading can be fixed at its average normal value.

An alternative to reconfiguring the matrix may be, to simply leave the sensor reading fixed at its average normal value. The redundancy of the system means that the error introduced will have only a small effect on the overall performance. However, there may occur large perturbations for which the average value is seriously in error. We have investigated this alternative approach to sensor failure and its response to large perturbations. We find that the system requires several sensor-actuator cycles to recover from a large perturbation when a sensor is fixed to read its average value. Each cycle however produces a factor of about 3 improvement in the fit so the number of cycles required to reconfigure the mirror is not large. Because of this it appears practical to handle defective sensors in an adequate fashion (until they can be repaired or replaced) by simply replacing the actual sensor reading by its nominal one. The virtue of this technique is that the relatively time consuming process of generating a new B matrix can be avoided. As discussed below it is expected the B matrix generation will require about 200 times as long as a normal correction cycle.

VII. REAL TIME CONTROL

The computations for the control system are of two types as described above. The longer process is the "inversion" for solving the coupled set of linear equations. This needs to be performed only occasionally when, for example, a sensor fails. The number of mathematical operations for this inversion scales as the number of sensors times the number of actuators squared ($288(162)^2$). The calculations for this paper were performed on a CDC 7600 computer which uses 140 ns of central processor time per multiplication. The inversion required a total of 12.5 seconds.

Given the inversion, the actuator movements needed to respond to a set of sensor readings are calculated with a single matrix multiplication. For the 7600 this required 58 milliseconds. This is sufficiently short to respond to the expected rate of perturbations of about 10 Hz.

VIII. SUMMARY

As the size of a telescope primary mirror is increased the mass of the mirror needed to maintain a given image quality increases enormously (as approximately the third power of the diameter). To avoid this tremendous scaling of the mass (and cost) of the mirror and its support structure mirror designs consisting of an assembly of many small segments have been proposed. The central challenge of these designs is the creation of an economical and reliable system to sense and control the orientations of the segments. A specific design employing hexagonally packed segments has been proposed for a new 10-meter telescope for the University of California. The interlocking character of the hexagonal geometry allows measurement of the mirror segment orientations with simple capacitive displacement sensors. Information from these capacitive sensors is then used to control the orientations of the segments and maintain the figure of the primary in response to perturbations of wind, gravity loading, and temperature changes.

We have made a computer analysis of such a control system. The program that would be used to actuate movement of the segments in response to the sensor information has been written. Using this program we have quantitatively established the effects of sensor and actuator noise on the image quality. The image size scales linearly with the rms errors in the sensors and actuators. For assumed values of 0.05 microns for each of these the resulting image gaussian widths are 0.065 and 0.034 arc seconds. Combined in quadrature these give a width of 0.072 arc seconds and thus 80% of the energy is contained in a circle of 0.13 arc second

radius. Based on initial estimates and tests of the sensors and actuators the assumed errors should be easily achieved. The resulting image size is well within the design goals of the 10-meter telescope and of course less than the atmospheric seeing for visible light. A diffraction analysis for the same assumed error levels shows the image will be diffraction limited at about 10 μm .

The program was also used to test the sensitivity of the system to sensor failures. For both random sets of failed sensors and for specific sets of sensors close to the reference mirror we found the image size degrades only very slowly with the sensors eliminated. This confirms our expectation that the sensor redundancy makes the control very stable.

In addition to investigating the image quality for the 10-meter telescope we have also studied the image quality as more segments are added. The size of image grows slowly enough that we conclude that the images from primary mirrors of even larger assemblies would not be degraded by sensor and actuator noise.

ACKNOWLEDGEMENTS

We wish to thank the telescope committee members: Joe Wampler, Harland Epps, Dave Rank, and Jack Welch for their critical comments. George Gabor was particularly helpful during the development of this method of control with ideas on the sensors and actuators. The exchange of various ideas for control of the segments with Larry Barr and other members of the Kitt Peak National Observatory NGT design group was also extremely helpful. The ideas, comments, and experience of Mike Reed of the MMT were of great value in assessing the likely precision and reliability of various sensors, actuators, and control schemes. We gratefully acknowledge the assistance of Uzi Arkadir and Ru-Mei Kung with the computer programming of the efficient algorithms. Finally we are happy to express our appreciation to David Saxon for his interest and generous support of the entire telescope project.

REFERENCES

1. Nelson, J., Optical Telescopes of the Future, Conference Proceedings, p. 133 (Dec 1977), Geneva 23: ESO c/o CERN 1978 "The Proposed University of California 10 Meter Telescope".
2. Nelson, J., Society of Photo-Optical Instrumentation Engineers Proceedings, Volume 172 (Jan 1979), "Segmented Mirror Design for a 10-Meter Telescope".
3. Crane, R., Optical Telescope Technology Workshop (April 1969), NASA Report SP-233 (page 297), "Figure Sensing Techniques".
4. See for example, Hardy, J.W. "The Role of Active Optics in Large Telescopes" in Optical Telescopes of the Future, Conference Proceedings, p. 455 (Dec 1977), Geneva 23: ESO c/o CERN 1978.
5. Gabor, G., Proceedings of the Society of Photo-Optical Instrumentation Engineers, Volume 172 (Jan 1979), "Position Sensors and Actuators for Figure Control of a Segmented Mirror Telescope".
6. Golub, G.H. and Reinsch, C., Numerische Mathematik 14, 403-420 (1970).
7. Born, M. and Wolf, E., Principles of Optics, 4th Edition Pergamon Press (1970).
8. Shack, R., in Kitt Peak National Laboratory Report (July 1977), "The NGT, Next Generation Telescope Report No. 3" page A-54.

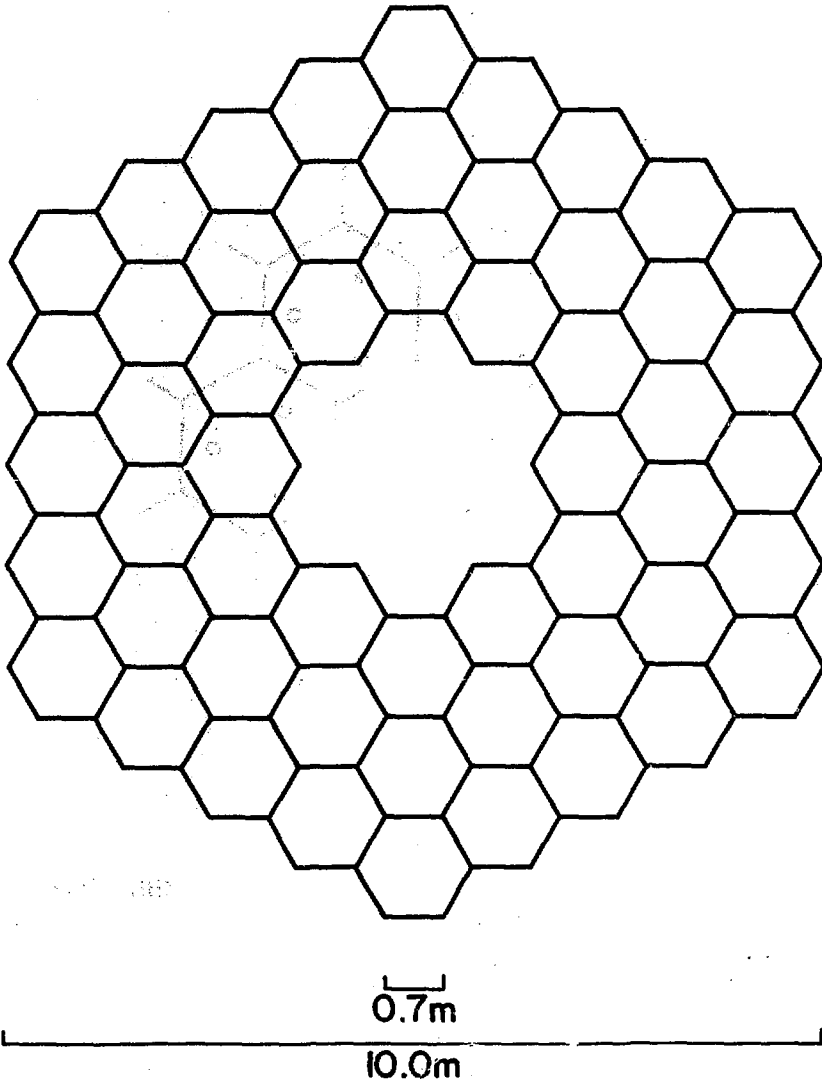
FIGURE CAPTIONS

1. The geometry of the central reference mirror and the surrounding three rings of 54 mirror segments. The area is equal to that of a 10-meter diameter circular mirror.
2. The location of some of the 162 actuators shown schematically on the backs of the mirror segments. The actuators control the orientation of the segments.
3. The position of the 288 displacement sensors used for sensing the relative orientations of the mirror segments.
4. Plan (a) and oblique (b) views of the central reference mirror and one mirror segment illustrating the displacements measured by the sensors.
5. Definition of the mirror segment types labeled by their degree of coupling through the sensors to the central reference mirror.
6. A typical image spot diagram generated by 0.05 μm of sensor noise. Each spot is the geometric image of a mirror segment.
7. The one dimensional gaussian width δ (arc seconds) of the image spot distribution as a function of the number of rings of segments included in the primary mirror.
8. The one dimensional gaussian width δ (arc seconds) of the image spot distribution for the segments of various types. Points for primary mirrors consisting of 1, 2, 3, and 4 rings of segments are shown.

9. The rms surface error (microns) for various mirror types.

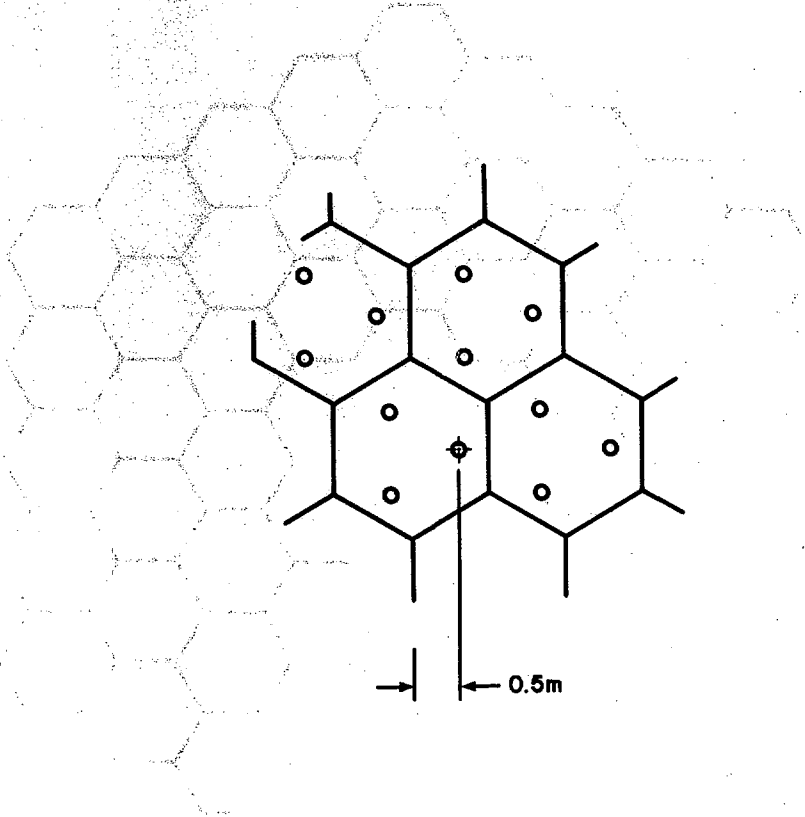
Points for primary mirrors consisting of 1, 2, 3, and 4 rings of segments are coincident.

10. The results of a diffraction calculation of the image resulting from $0.05 \mu\text{m}$ of sensor noise. The radius (arc seconds) of a circle in the image plane containing 80% of the energy versus wavelength (microns).



XBL 795-1572

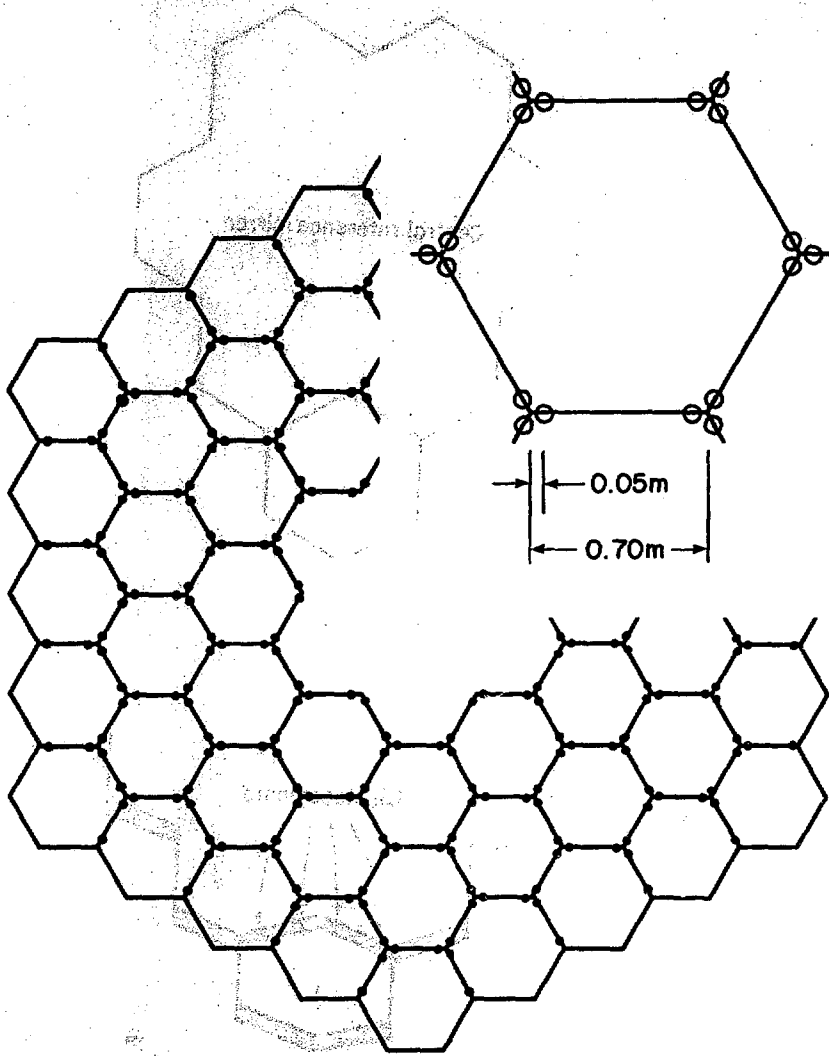
Fig. 1



XBL 795-1573

Fig. 2

5781-077



XBL 795-1574

8101-001 J02

Fig. 3

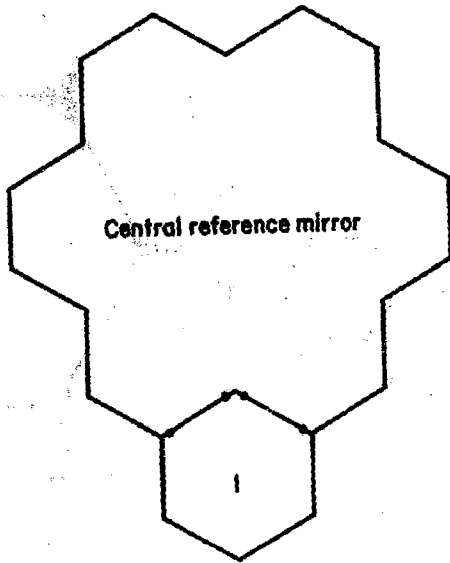


Fig. 4a

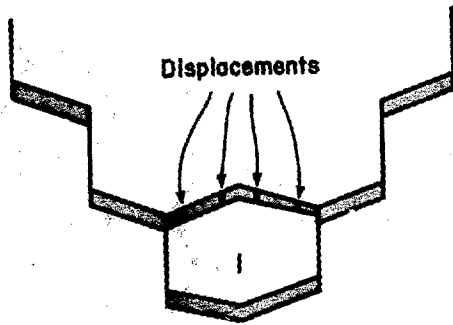
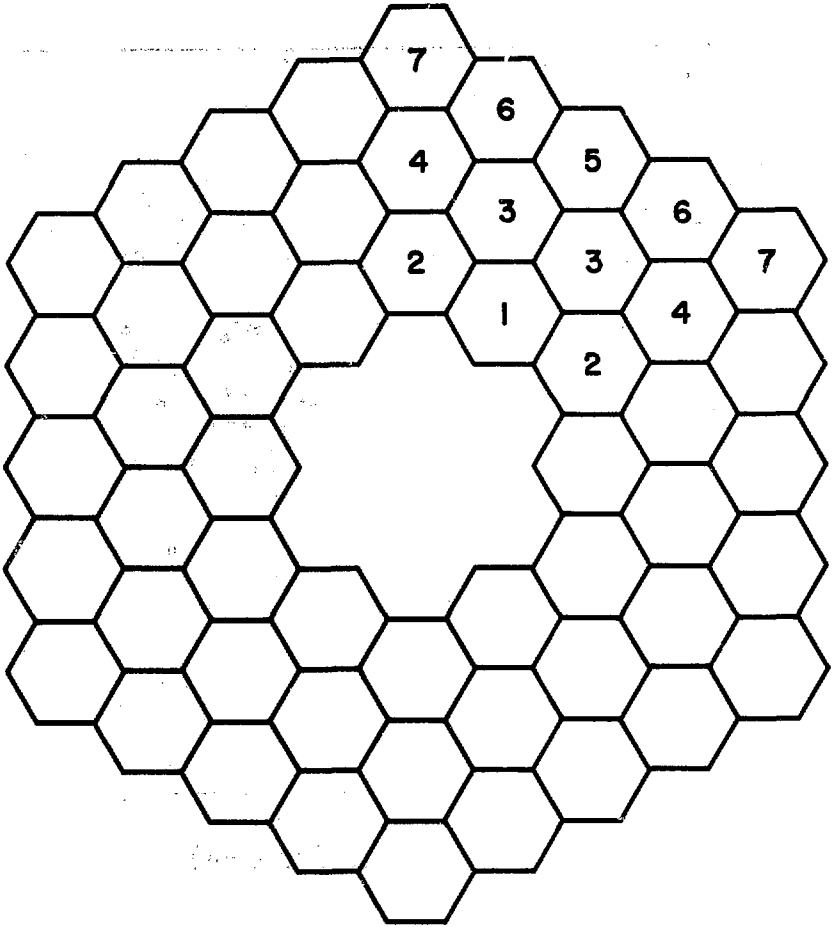


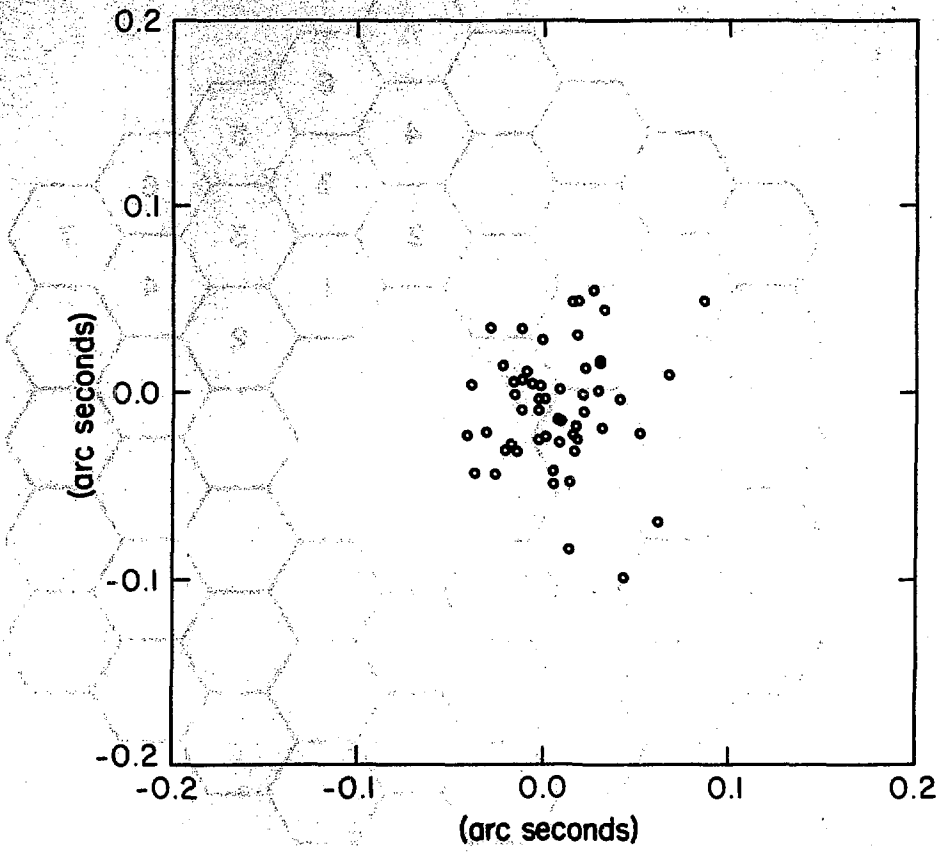
Fig. 4b

XBL 795-1575



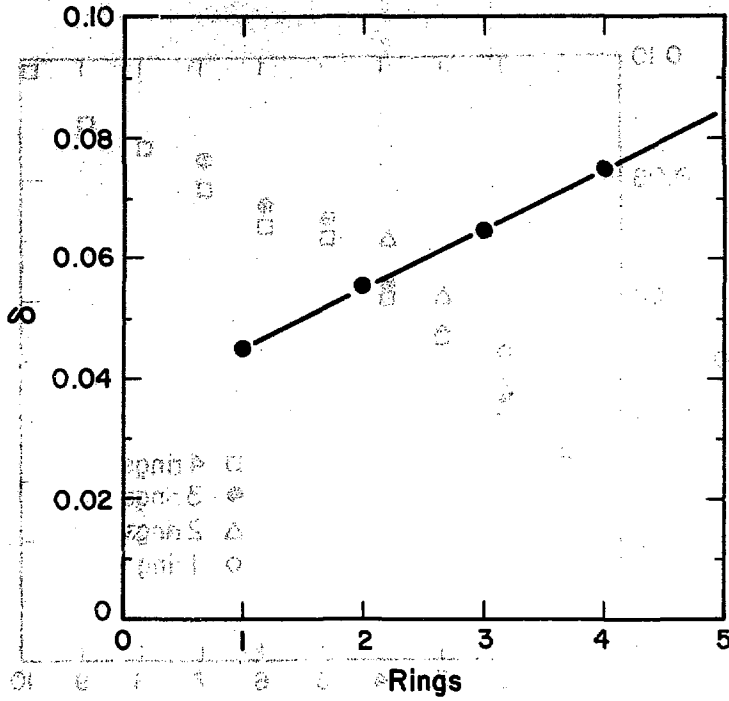
XBL 795-1576

Fig. 5



XBL 795-1577

Fig. 6

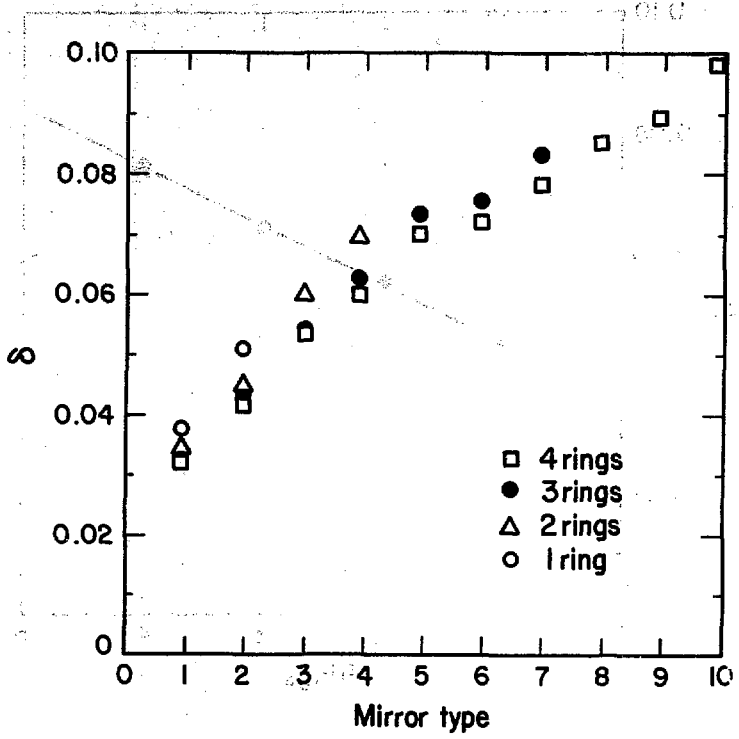


XBL 795-1578

0Y01-REV 100X

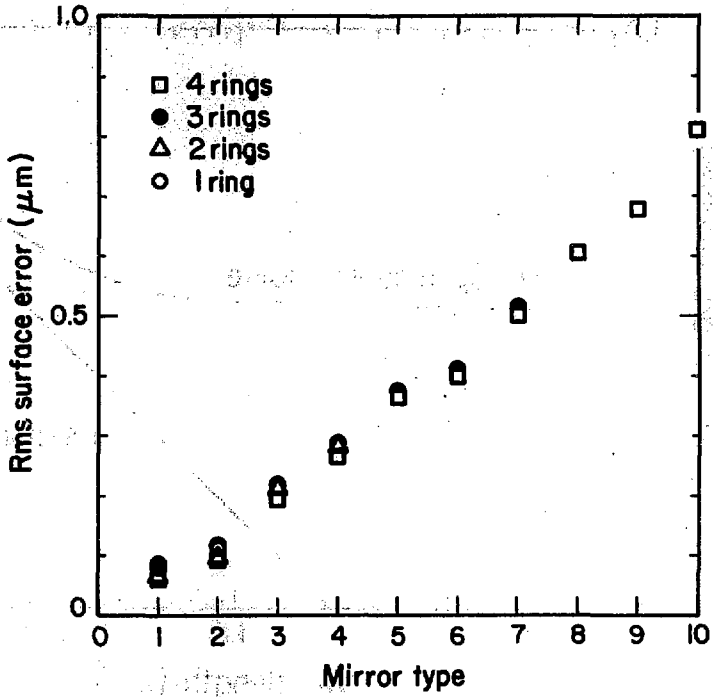
Fig. 7

0.017



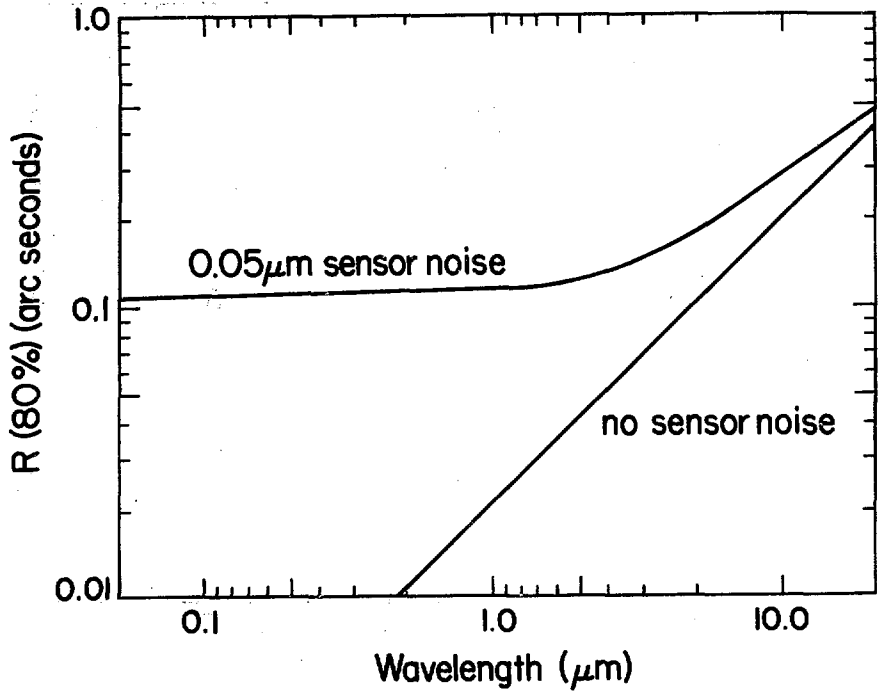
XBL 795-1579

Fig. 8



XBL 795-1580

Fig. 9



XBL 795 - 1581

Fig. 10